DOI: https://doi.org/10.14256/JCE.4468.2025

Građevinar 8/2026

Primljen / Received: 19.12.2025.
Ispravljen / Corrected: 29.4.2026.
Prihvaćen / Accepted: 18.5.2026.
Dostupno online / Available online: 10.9.2026.

Mechanical characteristics and parameter optimisation for extra-large deep foundation excavation at cross-transfer subway stations

Authors:

[4]Assoc.Prof. **Zhennan Liu**, PhD. CE
759179282@qq.com
Corresponding author

[1]Zhiquan Wang
[1]Feng Tian
[1]Heng Zhang
[1]Mingliang Tao
[1]Ningxiang Luo
[2]Zijian Wang
[3]Chenyang Liu
[4]Xingchao Tian

[1]Powerchina Railway Construction Investment Group CO., China
[2]Sinohydro Engineering Bureau 4 CO., China
[3]Sinohydro Engineering Bureau 7 CO., China
[4]University of Civil Engineering, Transportation and Water Conservancy
Guizhou Institute of Technology, Guiyang, China

Original research paper

Zhiquan Wang, Feng Tian, Heng Zhang, Mingliang Tao, Ningxiang Luo, Zijian Wang, Chenyang Liu, Zhennan Liu, Xingchao Tian

Mechanical characteristics and parameter optimisation for extra-large deep foundation excavation at cross-transfer subway stations

Strict control of ground settlement and internal forces within the support structure represents a key technical challenge in the excavation of extra-large deep-foundation pits for cross-transfer metro stations. Based on the field monitoring results of the research section and fundamental geotechnical parameters of the rock mass, two-stage excavation schemes, BZL1 and BZL2, are proposed. The model was validated against the monitoring data. The evolution patterns of the ground settlement and internal forces within the support system for the two excavation schemes were analysed, and the optimal excavation scheme was selected. The results showed that the maximum error between the numerical simulation and field monitoring data of the ground settlement under the BZL1 excavation scheme was 13.84 %, indicating that the established model was reliable. When the BZL2 scheme for excavating foundation pits was employed, the peak cumulative surface settlement could be reduced by up to 56.7 %, whereas the peak axial force in the cross braces could be reduced by up to 48.14 %. The BZL2 scheme is the preferred option for excavating ultradeep large-scale foundation pits, offering superior safety and economic viability. These findings may serve as a reference for the construction of extra-large deep excavations at cross-transfer underground railway stations.

Key words:

cross-transfer, metro station, extra-large deep foundation, mechanical properties, ground subsidence

Izvorni znanstveni rad

Zhiquan Wang, Feng Tian, Heng Zhang, Mingliang Tao, Ningxiang Luo, Zijian Wang, Chenyang Liu, Zhennan Liu, Xingchao Tian

Mehaničke karakteristike i optimizacija parametara pri iskopu vrlo velikih i dubokih građevinskih jama na križnim presjednim postajama metroa

Stroga kontrola slijeganja tla i unutarnjih sila u potpornoj konstrukciji predstavlja ključni tehnički izazov pri iskopu vrlo velikih i dubokih građevinskih jama na križnim presjednim postajama metroa. Na temelju rezultata terenskog monitoringa na istraživanoj dionici i osnovnih geotehničkih parametara stijenske mase predložene su dvije fazne sheme iskopa, BZL1 i BZL2. Model je validiran usporedbom s podacima monitoringa. Analiziran je razvoj slijeganja tla i unutarnjih sila u potpornom sustavu za obje sheme iskopa te je odabrana optimalna shema. Rezultati su pokazali da je najveće odstupanje između numeričke simulacije i terenskih podataka o slijeganju tla za shemu iskopa BZL1 iznosilo 13,84 %, što upućuje na prihvatljivu pouzdanost uspostavljenog modela. Primjenom sheme BZL2 najveće kumulativno slijeganje površine može se smanjiti do 56,7 %, a najveća se aksijalna sila u poprečnim podupiračima može smanjiti do 48,14 %. Shema BZL2 pokazala se prikladnijim rješenjem za iskop vrlo velikih i dubokih građevinskih jama jer osigurava višu razinu sigurnosti i povoljniju ekonomičnost izvedbe. Dobiveni rezultati mogu poslužiti kao smjernice za izvođenje vrlo velikih i dubokih iskopa na križnim presjednim postajama metroa.

Ključne riječi:

križna presjedna postaja metroa, metro, vrlo velika i duboka građevinska jama, mehanička svojstva, slijeganje tla

1. Introduction

Underground railways are a vital modern transport solution for alleviating urban traffic congestion and are capable of significantly improving the surface traffic conditions within cities. Banzhulin Station of Chongqing Rail Transit is a cross-shaped interchange station constructed for Lines 7 and 17. The excavation area of the foundation pit at Banzhulin Station exceeds 18,000 m², with a maximum excavation depth of 31.24 m. In accordance with the Technical Code for the Demolition of Enclosure Structures of Super-Large and Deep Foundation Pits (T/LCH 030-2025), it is classified as a super-deep and large-scale foundation pit. At this scale and depth, the mechanical behaviour of the rock and soil mass around the foundation pit no longer satisfies the basic assumptions of homogeneity, continuity, small deformation, and limit equilibrium, rendering classical mechanical models inapplicable [1–5]. Achieving active control of ground-surface settlement and structural disturbance for a "super-deep and large foundation pit plus cross-interchange" is an urgent, yet unsolved, technical problem. Therefore, investigating the mechanical properties of the surrounding soil for excavating exceptionally deep foundation pits for cross-transfer metro stations and optimising the excavation methods and parameters are of paramount importance for the safe and efficient construction of metro stations.

Numerous studies have been conducted on the mechanical response characteristics of metro foundation pit excavations. Zhang et al. [6] proposed internal force equations for the pile walls and joints of a dual-purpose wall structural system and analysed their mechanical properties. Chen et al. [7] analysed the influence patterns of excavation in soft soil foundations on adjacent underground railway crossings based on monitoring data. Wang et al. [8] employed numerical simulation methods to investigate disturbance influence zones and groundwater effects associated with cross-asymmetric excavations. Shi et al. [9] studied the evolution characteristics of soil and support structure deformation and axial support forces under different sectional excavation methods using a Wuhan metro station as a case study to determine a safe and economical excavation method. Li et al. [10] proposed that a delayed support scheme could be employed during the excavation of deep foundations in hard rock, thereby fully utilising the inherent stability of the rock mass and reducing construction costs. Liang et al. [11] investigated the intrinsic mechanisms of large deformations that occur during the excavation of deep underground railway pits using the tunnel front station method. Li et al. [12] examined the similarities and differences in the deformation characteristics between ultra-deep and conventional excavations and investigated reliable shoring methods. Ding et al. [13] employed model testing and numerical simulation methods to analyse the protective efficacy of isolation piles during underground railway excavation and investigated the optimal design parameters for such piles. Fu et al. [14] proposed a method employing compacted grouting to control horizontal deformation in underground railway excavations and optimised the grouting parameters based on the expansion theory. Ge et al. [15] developed a novel high-shear bolted active joint capable of significantly enhancing the compressive and tensile resistance of underground railway excavation pits. Qi et al. [16] employed numerical simulation methods to analyse the mechanical characteristics of excavations for deep foundation pits in super-large metro projects and optimised the support system based on an energy consumption analysis. The aforementioned research findings provide significant guidance for optimising excavation plans and support parameters for underground railway foundation pits. Cross-transfer stations situated at the junctions of multiple underground lines involve more complex excavation processes and mechanical response characteristics, necessitating further systematic research.

The impact of underground railway excavations on surrounding buildings and structures must be strictly controlled to ensure project safety. Chen et al. [17] proposed a protection technique for foundation pit excavation by which the maximum horizontal deformation was reduced by 43 %. Zhao et al. [18] analysed the impact patterns of asymmetric deep foundation pit excavation on adjacent underground railway stations and proposed an optimal excavation scheme. Zhang et al. [19] proposed the STdeep model to precisely predict the ground surface settlement for underground railway excavation pits. Wu et al. [20] proposed an intelligent multisource fusion evaluation model to achieve a comprehensive multi-indicator assessment of the safety status of underground railway excavation pits. Wei et al. [21] employed full-scale loading tests to investigate the mechanical response characteristics during the excavation process of a metro foundation pit, using the Hangzhou Metro as a case study. Xu et al. [22] utilised the Shanghai Metro deep foundation pit project as a case study to establish a long short-term memory neural network prediction model, thereby achieving accurate forecasting of building settlement during the excavation process. Liu et al. [23] employed numerical simulation methods to analyse the settlement behaviour of metro foundation pits during cut-and-cover backfilling excavation using Wuhan Metro Line 12 as a case study. Xu et al. [24] developed a prediction model for the deformation of retaining structures in deep excavations for underground railways based on a random forest model and found that the depth of the structure significantly influences the prediction of its deformation. Gao et al. [25] developed a three-dimensional nonlinear numerical model incorporating soil, structure, and interaction effects to investigate the influence of structural type and construction methods on the seismic performance of underground railway excavation pits. Dong et al. [26] established a horizontal displacement disaster model based on an adjusted log-periodic function model, enabling the accurate identification and early warning of vulnerable locations in retaining piles for metro excavation pits.

To achieve safe and economical excavation of super-large and deep foundation pits at cross-interchange metro stations, this study innovatively proposes a combined control method of "reserved core soil + symmetrical excavation". Its core principle is to actively retain the central rock column to suppress asymmetric disturbances in the unloading path of the surrounding rock, thereby overcoming the limitations of traditional graded-slope excavation or single-symmetrical excavation in controlling the interface stability of interbedded rock masses. To verify the superiority of this method, a systematic study was conducted using numerical simulations. First, rock and soil samples were collected from the research section onsite and processed into standard test specimens. Static tests were conducted to determine the basic mechanical parameters of the rock and soil mass and to perform parameter correction. Then, the FLAC3D numerical simulation software was used to establish a three-dimensional model for the excavation of the super-large and deep foundation pit at Banzhulin Station, and the model was verified using field monitoring data. Finally, the evolution laws of the surrounding soil settlement and internal force of the transverse bracing under different excavation and support sequences were analysed, and the optimal excavation scheme was selected. The proposed method ensures effective control of foundation pit deformation and safe and efficient construction. This method has not only achieved satisfactory results in practical engineering but also provides new theoretical insights for the design and construction of super-deep interbedded rock foundation pits.

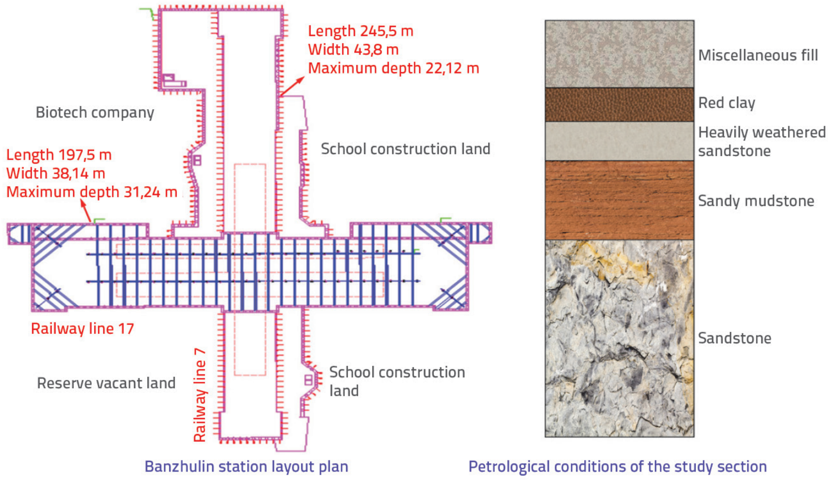

Figure 1. Plan view of Banzhulin station and the stratigraphic lithological conditions at its location

2. Project background

2.1. Project overview

Banzhulin Station is a cross-platform interchange station for Chongqing Rail Transit Lines 7 and 17. There is a biotechnology company to its northeast, school development land to its southwest and southeast, and a reserve plot to the northwest. Banzhulin Station on Line 7 spans a total length of 245.5 m, with a width of 43.8 m and a maximum depth of 22.12 m. It is a two-level (partially three-level) underground station featuring a double-column, three-span island platform configuration. Banzhulin Station on Line 17 spans a total length of 197.5 m, with a width of 38.14 m and a maximum depth of 31.24 m. It is a three-level underground station featuring a four-column, five-span side platform configuration. The stratigraphic lithology at Banzhulin Station comprises miscellaneous fill, red clay, heavily weathered sandstone, sandy mudstone, and sandstone, with construction employing the open-cut method. The plan view and lithological conditions of Banzhulin Station are shown in Figure 1. To comprehensively evaluate the mechanical response characteristics during deep foundation pit excavation at Banzhulin Station and its impact on the surrounding environment, the ground settlement and internal forces within the steel bracing systems were monitored and analysed. Ground settlement monitoring was conducted using a Trimble DiNi0.3 electronic level, whereas the internal forces within the steel supports were monitored using steel-string frequency axial-force transducers. The monitoring point layout is shown in Figure 2, and the ground settlement and internal force monitoring results for selected points are presented in Figure 3.

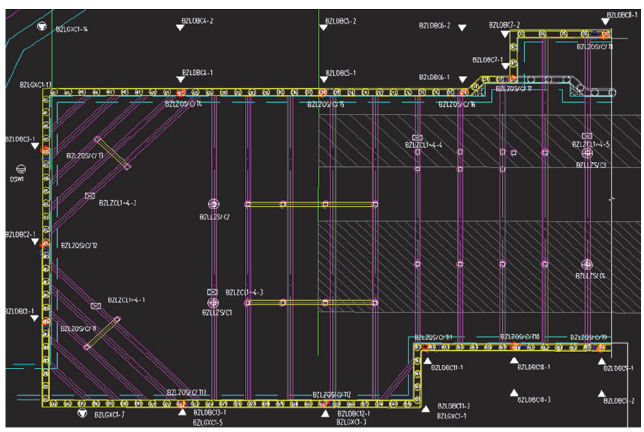

Figure 2. Layout of monitoring points for surface subsidence and internal forces in steel supports at Banzhulin Station

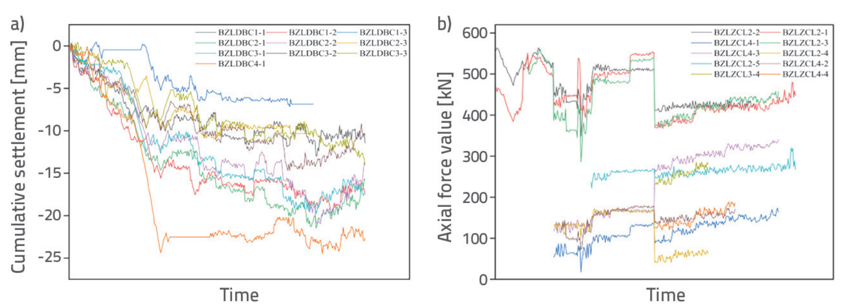

Figure 3. Monitoring results of surface settlement and internal forces in steel supports at Banzhulin Station: a) Ground subsidence; b) Internal forces in steel supports

As shown in Figure 3, surface subsidence was particularly pronounced at BZLDBC2-1 and BZLDBC4-1, with cumulative subsidence exceeding 20 mm. The internal forces within the steel supports at locations BZLZCL2-1, BZLZCL2-2, and BZLZCL2-3 were substantial, with maximum internal forces exceeding 550 kN. The field monitoring results indicate that, under the current excavation methodology, the internal forces acting on the support structure are substantial, with pronounced settlement observed in certain peripheral areas. Therefore, there is an urgent need to optimise and adjust the current deep excavation techniques to reduce internal stresses within the support structure, control excavation deformation, and ensure safe and efficient construction.

2.2. Testing of geotechnical physical parameters

The accurate determination of the fundamental mechanical parameters of the soil and rock mass within the section under study at the Banzhulin site is a prerequisite for adjusting the excavation methodology for the foundation pit. The soil layers in the study area exhibit good isotropy. Direct shear and triaxial tests were performed on the soil samples, with three specimens in each group. The basic mechanical parameters of the soil mass in the study area were obtained based on the geotechnical engineering investigation report for Banzhulin Station, as listed in Table 1.

The rock mass in the studied section exhibits a complex and variable lithology, with pronounced anisotropic properties. To accurately determine the mechanical parameters of the rock in the study area, strongly weathered sandstone, sandy mudstone, and sandstone were processed into standard cylindrical specimens with dimensions of 50 mm × 100 mm. The densities of the rock samples were measured using Vernier callipers and an electronic balance. Uniaxial and triaxial compression tests were conducted using RMT-301 rock and a concrete mechanical testing system. The test procedure employed a constant-displacement-rate loading control method with a loading rate of 0.005 mm/s. The confining pressures for the triaxial compression tests were set to 0, 5, 10, and 15 MPa. Uniaxial compression tests were conducted in triplicate for each rock type. Triaxial compression tests under each confining pressure were performed in duplicate. The final results were considered as the average values to minimise the effect of data discreteness on the test results. The static testing procedure for the rock samples is illustrated in Figure 4, and the fundamental mechanical parameters for the different rock types are listed in Table 1.

A rock mass consists of rock and discontinuous structural planes, and its strength and stiffness are significantly lower than those of intact rock. Therefore, it is necessary to further reduce the basic mechanical parameters of the rocks compared to those listed in Table 1. In this study, the geological strength index (GSI) system and the Hoek-Brown yield criteria were adopted to reduce the uniaxial compressive strength, elastic modulus, and cohesion [27, 28].

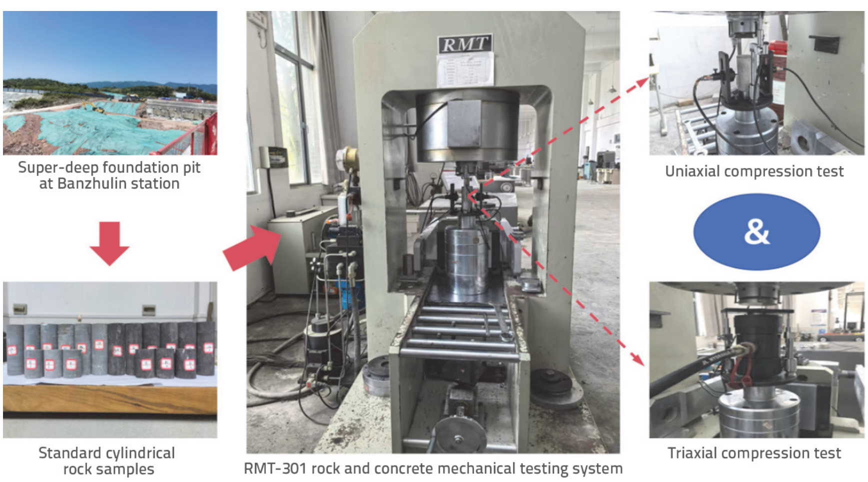

Figure 4. Static testing procedure for rock samples

Determining the *GSI* and disturbance parameter *D* is critical for the application of the Hoek-Brown criterion. Based on the Standard for Engineering Classification of Rock Masses (GB/T 50218-2014) and on-site geological investigation data, the on-site rock mass was classified as Grade IV. According to the qualitative *GSI* chart based on the Hoek-Brown criterion, combined with the blocky/crushed rock mass structure and general condition of the structural planes, the *GSI* value was determined to be 45. This value is consistent with the empirical range for Grade IV rock masses. Blasting or mechanical

Table 1. Fundamental mechanical parameters of geomaterials

Lithology	Density [g/cm³]	Uniaxial compressive strength [MPa]	Elastic modulusi [GPa]	Poisson ratio	Cohesive force [kPa]	Internal angle of friction [°]
Miscellaneous fill	2.05	/	0.01	0.30	5.0	25.0
Red clay	2.01	/	0.03	0.35	20.6	12.0
Heavily weathered sandstone	2.25	8.1	0.40	0.40	200.0	30.0
Sandy mudstone	2.56	18.5	1.21	0.38	564.0	29.2
Sandstone	2.49	25.0	3.87	0.22	1610.0	32.5

Table 2. Basic corrected mechanical parameters of the rock and soil mass

Lithology	**Density** [g/cm³]	**Uniaxial compressive strength** [MPa]	**Elastic modulusi** [GPa]	**Poisson ratio**	**Cohesive force** [kPa]	**Internal angle of friction** [°]
Miscellaneous fill	2.05	/	0.78	0.30	1.0	25.0
Red clay	2.01	/	2.34	0.35	4.0	12.0
Heavily weathered sandstone	2.25	0.15	31.2	0.40	40.0	30.0
Sandy mudstone	2.56	0.34	94.4	0.38	113.0	29.2
Sandstone	2.49	0.46	302.0	0.22	322.0	32.5

excavation is often adopted for metro foundation pits, and a value of 0.7 is recommended for the disturbance parameter *D*. The rock mechanical parameters were corrected to rock mass mechanical parameters using the formulas recommended by Hoek-Brown, as shown in Equations (1) and (2):

$$\sigma_{cm} = \sigma_{ci} \cdot s^{a} \tag{1}$$

$$E_{rm} = E_i \cdot \left(0.02 + \frac{1 - D/2}{1 + e^{(60+15D-GSI)/11}}\right) \tag{2}$$

where σ_{cm} and E_{rm} represent the corrected rock mass compressive strength and elastic modulus, respectively. σ_{ci} and E_i represent the compressive strength and elastic modulus of intact rock, respectively. *s* and *a* are Hoek-Brown constants.

$$s = \exp\left(\frac{GSI - 100}{9 - 3D}\right) \tag{3}$$

$$a = 1/2 + 1/6 \cdot (e^{-GSI/15} - e^{-20/3}) \tag{4}$$

To reduce cohesion, RocLab software (Rocscience) was used for the calculation, and the parameters σ_{ci}, m_i, *GSI*, and *D* were input. The corrected mechanical parameters of the rock and soil masses are listed in Table 2.

3. Model development and parameters validation

3.1. Model establishment

FLAC3D finite difference software was employed to establish a three-dimensional model of the excavation of an exceptionally deep foundation pit at Banzhulin Station. The optimal excavation scheme was selected by analysing the settlement patterns of the surrounding soil and the evolution of the internal forces within the steel crossbracing under different excavation and support sequences. The length-to-width ratios of the foundation pits for Lines 17 and 7 are greater than five, indicating that they are elongated foundation pits. The geological conditions along the excavation length of the foundation pit are identical. Based on the plane strain assumption, a typical central section (excavation length of 60 m) was selected for the numerical simulation analysis. The length, width, and depth of the foundation pit excavation at Banzhulin Station for Line 17 are 60.00 m, 38.14 m and 31.24 m, respectively, and those for Line 7 are 60.00 m, 43.8 m and 22.12 m, respectively. In accordance with geotechnical engineering modelling standards, the overall dimensions of the model should be at least three to five times the excavation span. To balance the computational accuracy and efficiency, the length, width, and depth of the overall model were set to 180 m, 180 m and 100 m, which are 3.0, 4.1, and 3.2 times the maximum spans, respectively. The model base was set with fully fixed boundary constraints, a model surface with free boundaries and the remaining planes with normal boundary constraints. Each layer of rock and soil was modelled as a homogeneous material, and calculations were performed using the Mohr-Coulomb failure criterion. The gable beam support was modelled using SHELL elements, whereas the retaining piles and cross-braces were modelled using CABLE elements. The model mesh employed hexahedral elements comprising 124,252 elements and 85,321 nodes. The model parameters for the gable beam, cross-braces, and pile foundations are listed in Table 3. The three-dimensional numerical simulation model is shown in Figure 5.

Here, the reasons for neglecting the time effect when adopting the Mohr-Coulomb model are explained. First, the service life of foundation pit engineering is much shorter than that of permanent

Table 3. Parameters of the gable beam, cross-brace and pile foundation model

Materials	**Density** [g/cm³]	**Elastic modulus** [GPa]	**Poisson ratio**
Gable beam	2.4	32	0.2
Concrete cross-brace	2.4	32	0.2
Steel cross-brace	7.85	200	0.2
Pile foundation	2.4	25	0.2

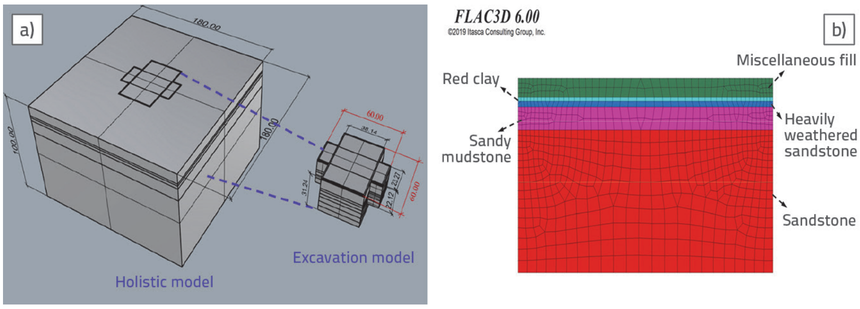

Figure 7. Three-dimensional simulation model of crown beam and cross brace

underground structures such as tunnels. The excavation and support period of super-large and deep foundation pits for metro projects is typically 6–18 months, whereas the significant creep of mudstone usually requires several years or even longer to produce non-negligible deformation. Second, foundation pit excavation is a dynamic process involving staged unloading rather than a condition of constant load. In contrast to the constant load used in traditional creep tests, the stress path of the surrounding rock during foundation pit excavation is characterised by staged unloading, with support implemented immediately after each stage of unloading. Under such intermittent unloading-support cycles, creep deformation can be partially completed during the holding period of each load stage and masked by subsequent excavation disturbances. Third, this study adopts an excavation scheme of compartmentalised symmetrical excavation combined with reserved core soil. The time-dependent deformation of the surrounding rock is effectively restrained by actively controlling the unloading path and providing timely support. In summary, although mudstone exhibits rheological properties, the influence of the time effects can be reasonably neglected under the specific engineering conditions used in this study (short construction period and staged unloading with timely support).

The excavation and shoring sequence significantly influences the deformation and mechanical response characteristics of super-large deep excavations. Therefore, two excavation simulation models, BZL1 and BZL2, were established to investigate the deformation and mechanical response characteristics and optimise the excavation scheme.

The BZL1 scheme is shown in Figure 6(a). The specific excavation process is as follows. Excavate 1.3 m of rock and soil in area ① of Line 7, construct pile foundations, crown beams and concrete cross-bracing. Excavate 8.37 m of rock and soil in area ① of Line 7 and install steel cross-bracing. Simultaneously excavate 1.3 m of rock and soil in area ②, and construct pile foundations, crown beams and concrete cross-bracing. Excavate 7.95 m of rock and soil in area ① of Line 7 and install steel cross-bracing. Simultaneously excavate 8.37 m of rock and soil in area ② and install steel cross-bracing. Simultaneously excavate 1.3 m of rock and soil in area ③ of Line 7 while constructing pile foundations, crown beams and concrete cross-bracing. Excavate 4.5 m of rock and soil in area ① of Line 7 and install steel cross-bracing. Simultaneously excavate 7.95 m of rock and soil in area ② and install steel cross-bracing. Simultaneously excavate 8.37 m of rock and soil in area ③ of Line 7 and install steel cross-bracing. Excavate the remaining 9.12 m of rock and soil in area ① of Line 7. Simultaneously excavate 4.5 m of rock and soil in area ② and install steel cross-bracing. Simultaneously excavate 7.95 m of rock and soil in area ③ of Line 7 and install steel cross-bracing. Excavate the remaining 9.12 m of rock and soil in area ②. Simultaneously excavate 4.5 m of rock and soil in area ③ of Line 7 and install steel cross-bracing. Excavate the remaining 9.12 m of rock and soil in area ③ of Line

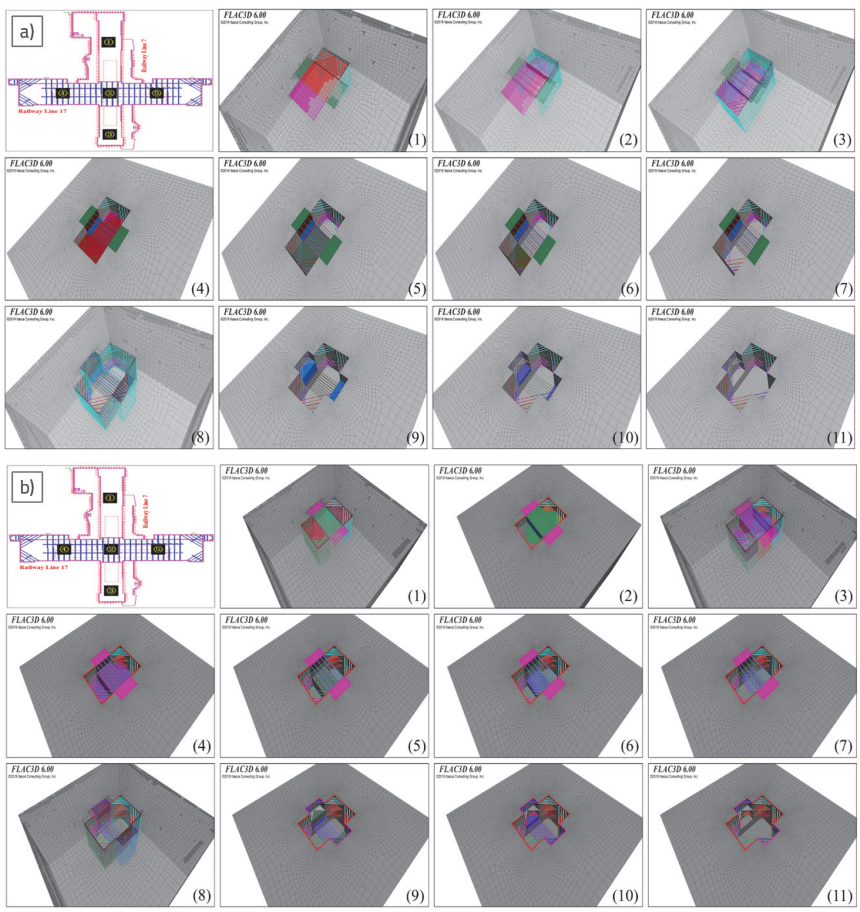

Figure 6. Excavation processes for the BZL1 and BZL2 programmes: a) BZL1 programme; b) BZL2 programme

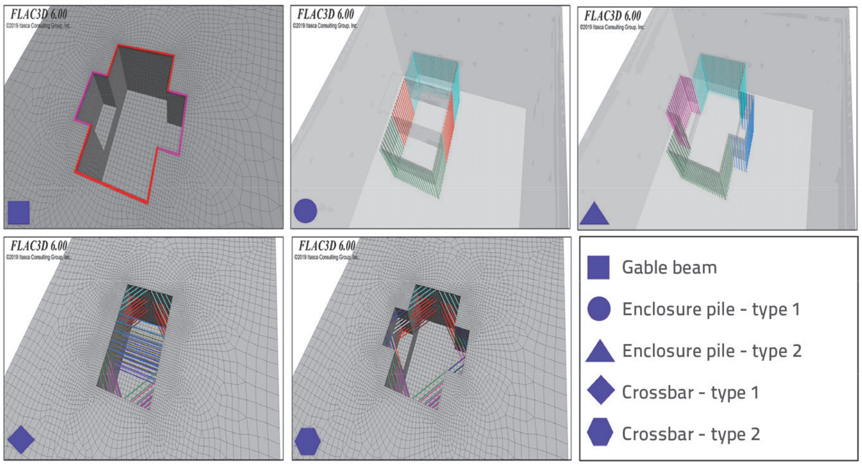

Slika 7. Trodimenzionalni simulacijski model krunske grede i poprečnih podupirača

7. Simultaneously excavate 1.3 m of rock and soil in areas ④ and ⑤ of Line 17, while constructing pile foundations, crown beams, and concrete cross-bracing. Remove the first layer of concrete cross-bracing in area ②. Simultaneously excavate 8.37 m of rock and soil in areas ④ and ⑤ of Line 17 while installing steel cross-bracing. Remove the second layer of steel cross-bracing in area ②. Simultaneously excavate 7.95 m of rock and soil mass in areas ④ and ⑤ of Line 17, installing steel cross-bracing. Remove the third layer of steel cross-bracing in area ②. Simultaneously excavate the remaining 4.5 m of rock and soil in areas ④ and ⑤ of Line 17, installing steel cross-bracing. Remove the fourth layer of steel cross-bracing in area ②.

The BZL2 scheme is illustrated in Figure 6(b). The specific excavation process is as follows. Simultaneously excavate 1.3 m of rock and soil in areas ① and ③ of Line 7 while constructing pile foundations, crown beams and concrete cross-bracing. Excavate 8.37 m of rock and soil in areas ① and ③ of Line 7 and install steel cross-bracing. Excavate 7.95 m of rock and soil in areas ① and ③ of Line 7 and install steel cross-bracing. Simultaneously excavate 1.3 m of rock and soil in area ②, and construct pile foundations, crown beams and concrete cross-bracing. Excavate 4.5 m of rock and soil in areas ① and ③ of Line 7 and install steel cross-bracing. Simultaneously excavate 8.37 m of rock and soil in area ② and install steel cross-bracing. Excavate the remaining 9.12 m of rock and soil in areas ① and ③ of Line 7. Simultaneously excavate 7.95 m of rock and soil in area ② and install steel cross-bracing. Excavate 4.5 m of rock and soil in area ② and install steel cross-bracing. Excavate the remaining 9.12 m of rock and soil in area ③ of Line 7. Simultaneously excavate 1.3 m of rock and soil in areas ④ and ⑤ of Line 17 while constructing pile foundations, crown beams, and concrete cross-bracing. Remove the first layer of concrete cross-bracing in area ②. Simultaneously excavate 8.37 m of rock and soil in areas ④ and ⑤ of Line 17 while installing steel cross-bracing. Remove the second layer of steel cross-bracing in area ②. Simultaneously excavate 7.95 m of rock and soil mass in areas ④ and ⑤ of Line 17 and install steel cross-bracing. Remove the third layer of steel cross-bracing in area ②. Simultaneously excavate the remaining 4.5 m of rock and soil in areas ④ and ⑤ of Line 17 and install steel cross-bracing. Remove the fourth layer of steel cross-bracing in area ②. The three-dimensional simulation model of the crown beam and cross brace is shown in Figure 7.

The primary difference between the BZL1 and BZL2 excavation programmes lies in the differing excavation sequence from area ① to area ③. In the BZL1 scheme, excavation is performed sequentially in the order of area ①, area ②, and area ③, with support provided. For the BZL2 scheme excavation, the rock and soil mass in reserved area ② is excavated after completing the excavation and supporting works for areas ① and ③.

To conduct a comparative analysis of the mechanical properties under the two excavation schemes, the ground settlement around the excavation perimeter and the axial forces in the crossbracing must be determined. It should be noted that the stress analysed in this study refers to effective stress. The layouts of the measurement points are shown in Figures 8 and 9. Figure 8 shows the 12 monitoring lines established for ground subsidence monitoring, with six monitoring points deployed along each line. The spacing between each measuring point was 3, 3, 5, 8, and 10 m. Measurement point 1 was used as an example. The distance between survey points 1-1, 1-2, and 1-3 was 3 m. The distance between survey points 1-3 and 1-4 was 5 m. The distance between survey points 1-4 and 1-5 was 8 m. The distance between survey points 1-5 and 1-6 was 10 m. Figure 9 shows the axial forces in the four layers of the cross-bracing. The first layer featured 25 monitoring points, whereas the second to fourth layers each contained 33 monitoring points. The positioning of the axial force monitoring points for the third-level cross-bracing remained consistent with that of the second level.

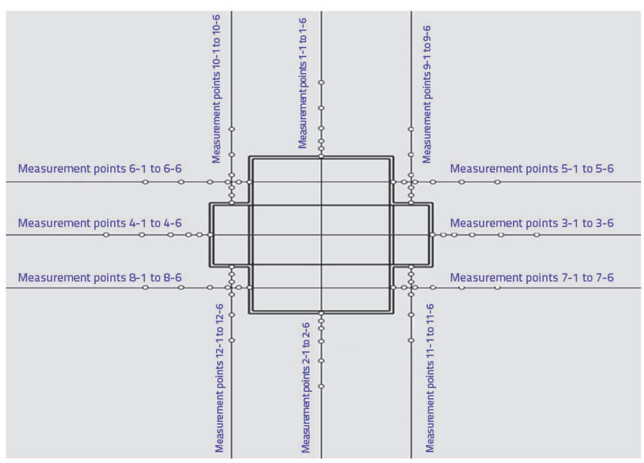

Figure 8. Schematic of monitoring point layout for surface settlement around the excavation pit

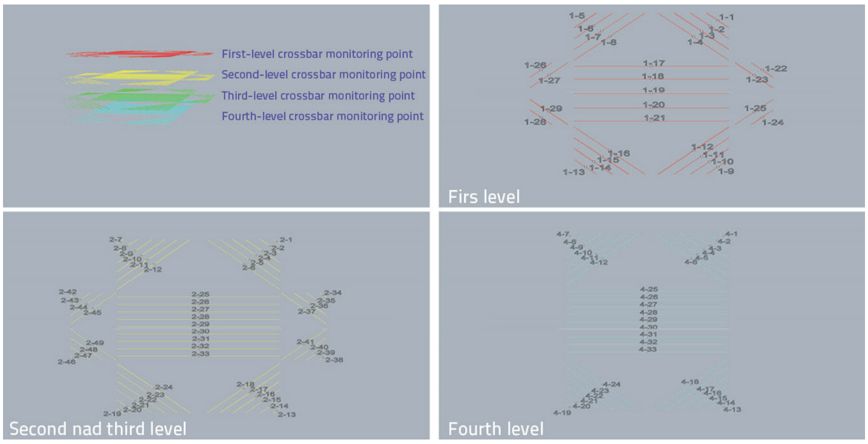

Figure 9. Schematic of monitoring point layout for transverse support axial force

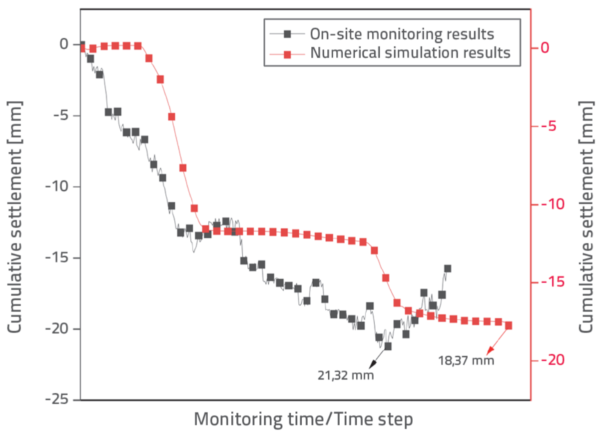

Figure 10. Validation results for the model and parameters

3.2. Model and parameters validation

To validate the reliability of the model and parameters, a comparative analysis was conducted between the numerical simulation results and the field monitoring data. In both excavation schemes, BZL1 and BZL2, first, the rock and soil mass in area ① of Line 7 is excavated. However, it should be noted that the BZL2 scheme requires the simultaneous excavation of the rock and soil mass in area ③. Therefore, the monitoring results obtained during excavation of the rock and soil mass in area ① of Line 7 under the BZL1 scheme were employed for model validation. The numerical simulation and field-monitoring results are shown in Figure 10. The variation trends of cumulative settlement obtained from numerical simulation and on-site monitoring are consistent. The maximum cumulative settlements from on-site monitoring and numerical simulation are 21.32 mm and 18.37 mm, respectively, with an error of 13.84 % between the two. The above analysis results indicate that the model and its parameters are reliable for predicting ground surface settlement under the excavation conditions of Scheme BZL1 [29]. Further analysis was conducted to determine the causes of the relatively large errors in the numerical simulation results. First, during onsite construction, changes in the groundwater level directly alter the effective stress in the soil, resulting in additional settlement of the surrounding structures. However, the effect of water pressure variations on surface settlement was not considered in the numerical simulation, resulting in lower values than the corresponding actual field measurements. Second, although the rock and soil masses were stratified in the numerical simulation, the material model and parameters within each layer were uniform. In their natural state, rock and soil masses exhibit anisotropy and heterogeneity, which are important sources of error. In addition, the excavation method in the numerical simulation is static, whereas actual construction is often accompanied by dynamic disturbances. Under dynamic disturbances, the ground surface typically undergoes significant settlement changes.

4. Analysis of results

4.1. Ground subsidence

The displacement contour plots for each excavation phase generated after the completion of the excavation and support works under the BZL1 scheme are shown in Figure 11, while the cumulative settlement patterns at each monitoring point are depicted in Figure 12. The analysis in Figure 12 reveals that settlement is most pronounced at monitoring points 2 and 3

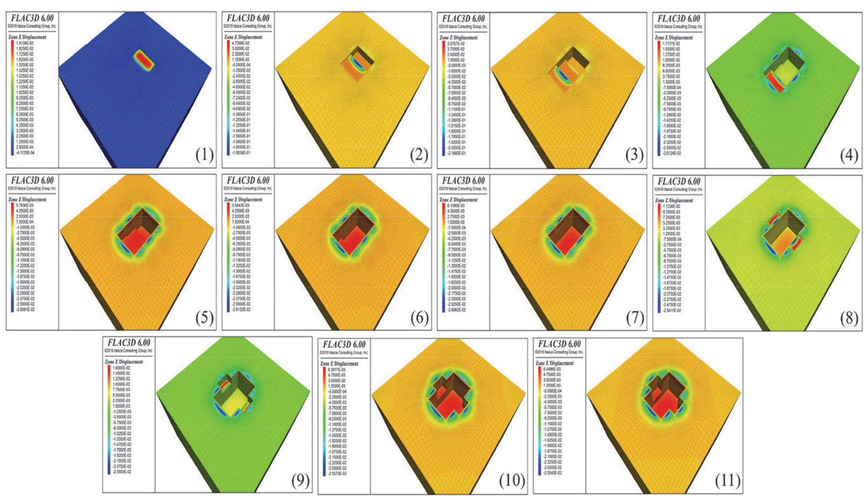

Figure 11. Displacement contour plots for each excavation step

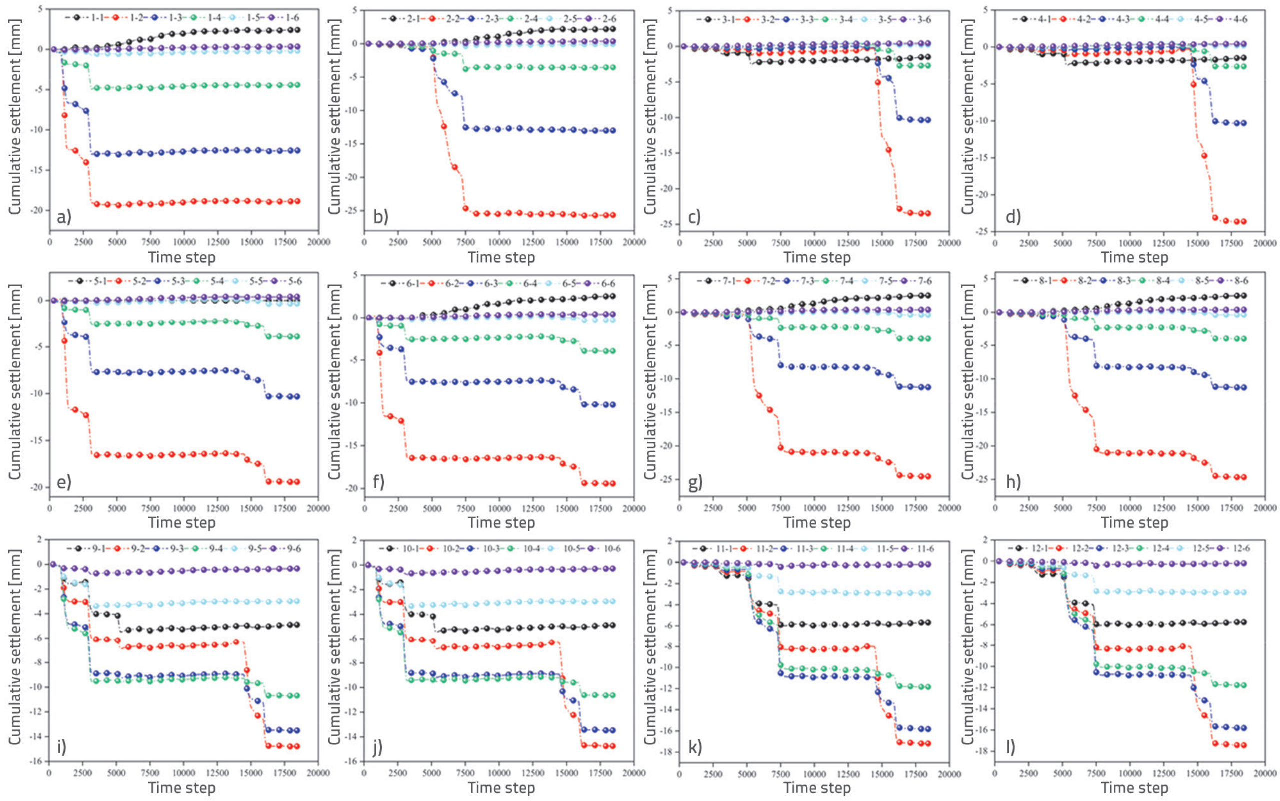

Figure 12. Cumulative settlement patterns at various monitoring points for the BZL1 scheme

along each survey line, indicating that this excavation scheme will impact structures within an 11 m radius of the excavation perimeter. The settlement at survey point 1 along each survey line was not significant and exhibited a slight upward bulging tendency. This was because test point 1 was situated on the excavation face. As the support was installed immediately after excavation, the support system compacted and densified the rock and soil at the test point, resulting in minimal settlement or even uplift owing to compaction. However, the settlement at monitoring point 1 along monitoring lines 9–12 was relatively pronounced. This is because, when areas ① and ② of Line 7 were excavated in sequence, the rock and soil mass at monitoring point 1 had not yet been supported. Once the excavation and support were completed, the settlement ceased to increase. Additionally, compared to other survey lines, the settlement at survey point 4 on survey lines 9–12 showed an increasing trend. This is because test point 4 on test lines 9–12 is situated at a crossroads area, where the rock and soil mass have been subjected to cyclic excavation disturbances, resulting in a slight increase in settlement.

To further analyse the location of the maximum settlement for the BZL1 scheme, the cumulative settlement peaks at survey points 2 and 3 along each survey line were examined, as shown in Figure 13. The cumulative settlement at survey point 2 across all survey lines exceeded 14 mm, with the maximum cumulative settlement reaching 25.54 mm. The cumulative settlement at measurement point 3 on each profile exceeded 10 mm, with a maximum cumulative settlement of 15.82 mm. The maximum cumulative settlement at survey point 2 occurred along survey lines 2, 7, and 8, whereas the maximum cumulative settlement at survey point 3 occurred along survey lines 11 and 12. As shown in Figure 5, when the foundation pit is excavated using the BZL1 scheme, significant surface settlement occurs around area ③ of Line 7, necessitating enhanced monitoring and early warning measures.

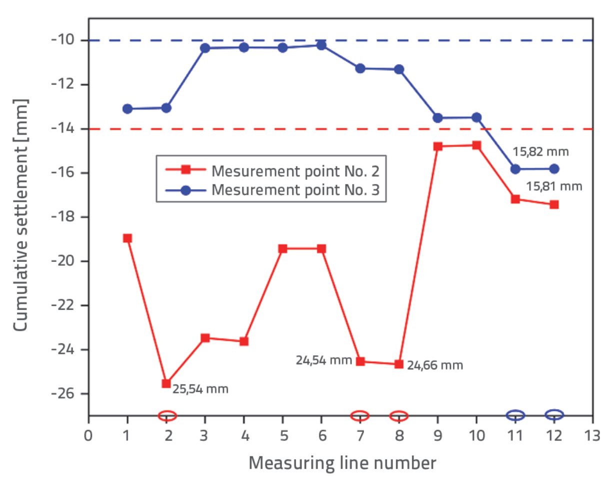

Figure 13. Peak cumulative settlement values at survey points 2 and 3 along each survey line

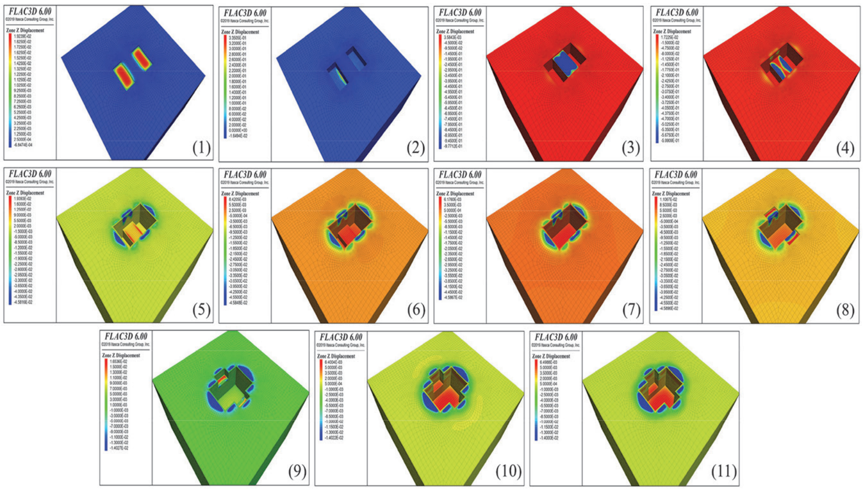

Figure 14. Displacement contour plots for each excavation step

The displacement contour plots for each excavation phase generated after the completion of the excavation and support works under the BZL2 scheme are shown in Figure 14, whereas the cumulative settlement patterns at each monitoring point are depicted in Figure 15. The cumulative settlement patterns for survey lines 1, 2, 3, 4, 5 to 8, and 9 to 12 were essentially consistent. This is attributable to the BZL2 scheme, which employs a symmetrical excavation approach coupled with the provision of reserved rock-soil sections at intersections. The analysis in Figure 15 reveals that settlement is most pronounced at survey point 2 along each survey line, indicating that this excavation scheme will impact structures within a 6 m radius of the excavation perimeter. Compared with the BZL1 excavation scheme, the BZL2 excavation scheme causes less disturbance to the surrounding environment of the foundation pit. The settlement at survey point 3 along survey lines 1 and 2, as well as survey lines 9–12, was relatively significant. This is because the excavation area for Line 7 was extensive, and when the rock and soil mass in areas ① and ③ of Line 7 were excavated, the unloading effect on the rock and soil mass was significant. Consequently, significant settlement occurred at survey point 3 along survey lines 1 and 2. The significant settlement at monitoring point 3 along survey lines 9 to 12 was caused by the lack of support at this location during the excavation of the rock and soil mass in areas ① and ③ of Line 7. The rock and soil mass at survey lines 1 and 2, as well as at survey point 1 on survey lines 5 to 8, exhibited a slight upward bulging tendency. This is due to the immediate shoring of the rock and soil mass in areas ① and ③ of Line 7 following excavation, which compacted the rock and soil mass at the measurement points. In contrast, the settlement

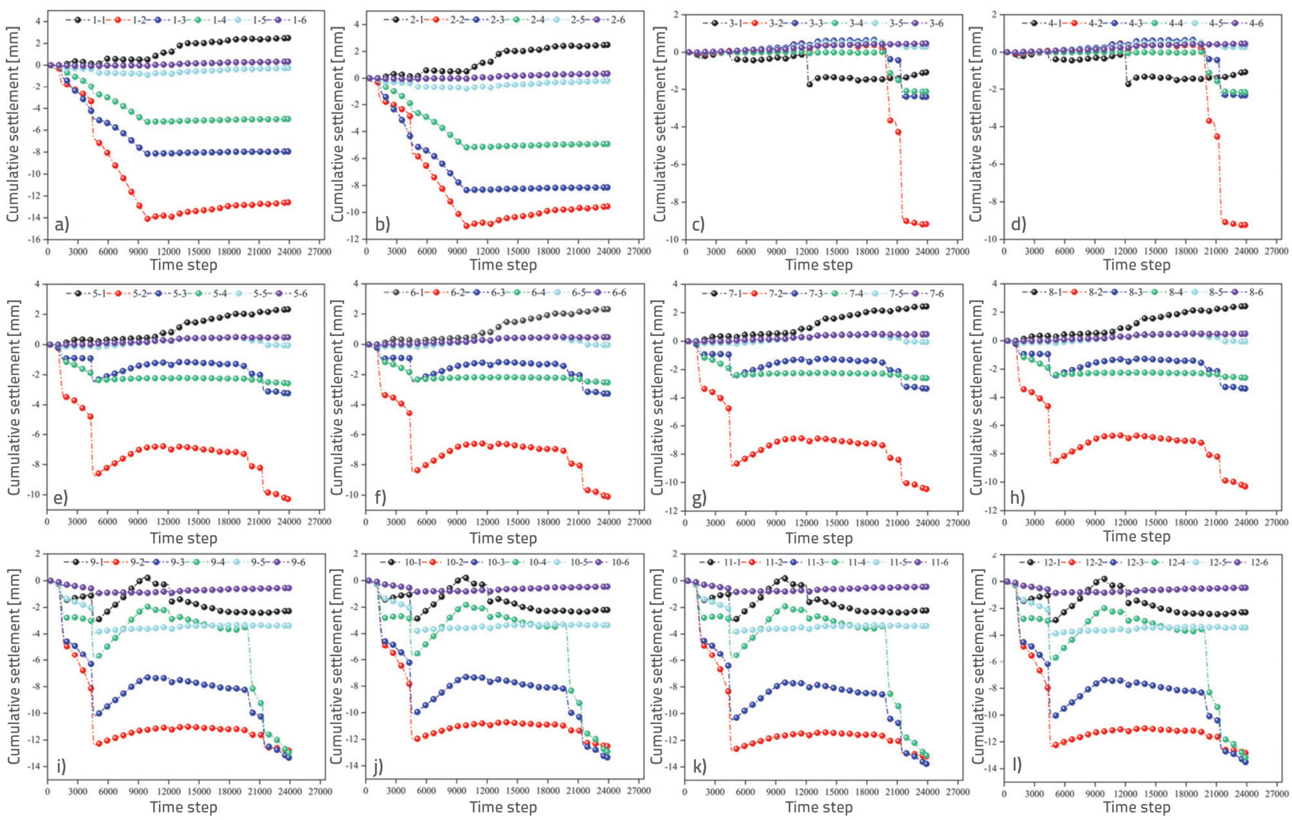

Figure 15. Cumulative settlement patterns at various monitoring points for the BZL2 scheme

at survey point 1 along survey lines 3 and 4, as well as survey lines 9 to 12, was relatively more pronounced. This is because, during the excavation of areas ① and ③ of Line 7, the rock and soil mass at monitoring point 1 had not yet been supported. Once the excavation support was completed, settlement ceased to increase. Additionally, the settlement at survey point 4 along survey lines 1 and 2, as well as survey lines 9 to 12, exhibited an increasing trend compared to that at other survey lines.

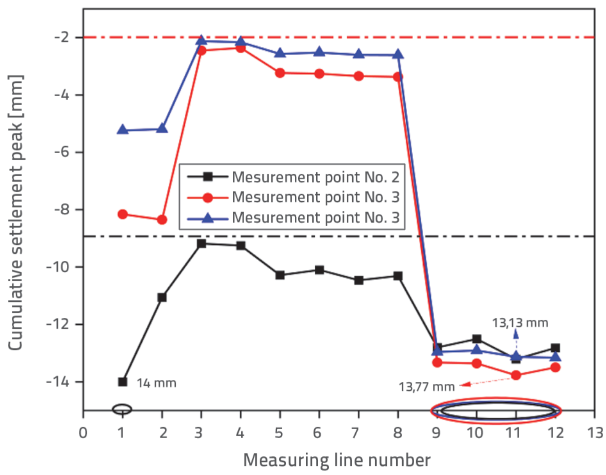

Figure 16. Peak cumulative settlement values at survey points 2 to 4 along each survey line

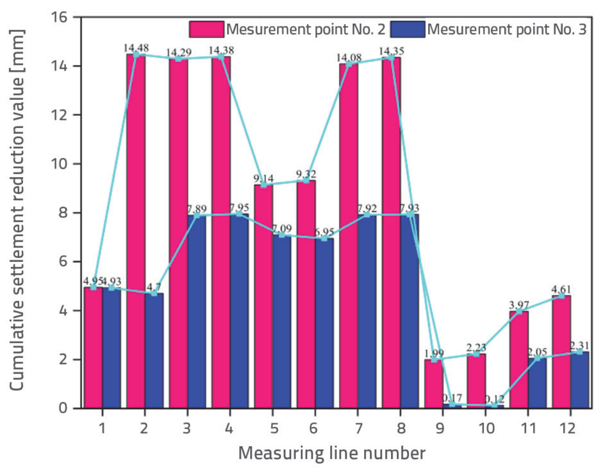

Figure 17. Cumulative settlement reduction value of scheme BZL2 relative to BZL1

To further analyse the locations of maximum settlement for the BZL2 scheme, the cumulative settlement peaks at survey points 2 to 4 along each survey line were examined, as shown in Figure 16. The cumulative settlement at survey point 2 across all survey lines exceeded 9 mm, with the maximum cumulative settlement reaching 14 mm. The cumulative settlements at monitoring points 3 and 4 along each profile exceeded 2 mm, with maximum cumulative settlements of 13.77 mm and 13.13 mm, respectively. The maximum cumulative settlement at monitoring point 2 occurred along survey lines 1 and 9 to 12. The maximum cumulative settlement at monitoring points 3 and 4 occurred along survey lines 9–12, respectively. As shown in Figure 6, when the foundation pit was excavated using the BZL2 scheme, significant surface settlement occurred around areas ① and ③ of Line 7, necessitating enhanced monitoring and early warning measures.

A comparative analysis of the cumulative settlement peaks for survey lines 2 and 3 under schemes BZL1 and BZL2 is shown in Figure 17. The vertical axis represents the cumulative reduction in the settlement under BZL2 relative to that under BZL1. Adopting the BZL2 scheme to excavate the foundation pit can reduce the peak cumulative settlement by up to 56.7 % compared to that under the BZL1 scheme, demonstrating superior control over foundation pit deformation. When the BZL2 scheme was used to excavate the foundation pit, the surface settlement of the structures built near survey lines 2–8 was reduced significantly.

4.2. Internal forces in support structures

The variation patterns of the transverse support axial forces at each monitoring point obtained after the completion of the excavation and support works are illustrated in Figure 18 for both schemes. As excavation progresses, the axial force in the crossbracing generally exhibits an increasing trend initially before stabilising. Steps 1 to 7 of both excavation schemes involve excavating the surrounding rock and soil around Line 7, while steps 8 to 11 involve excavating the surrounding rock and soil around Line 17. Following the initial excavation, pile foundations, crown beams, and concrete crossbracing were installed. At this stage, the axial force acting on the concrete crossbracing reached its maximum value. The rock and soil surrounding Line 7 were excavated up to the sixth step, at which point the axial force on the cross-bracing was at its minimum. As the excavation commenced around Line 17 in step 8, the axial force within the cross-braces increased owing to the support provided to the surrounding rock and soil mass, resulting in a tendency for the axial force in the cross-braces to rise. The excavation procedures for steps 8 to 11 are identical for both schemes. Therefore, the variation patterns of the transverse support axial force were essentially consistent. As shown in Figure 18(a), the maximum axial force in the cross-bracing under the BZL1 scheme occurred during the first excavation phase, reaching a peak value of 512.14 kN. The minimum axial force in the cross braces occurred during the tenth excavation phase, with a minimum axial force of 198.1 kN. As shown in Figure 18(b), the maximum axial force in the cross-bracing under the BZL2 scheme also occurs during the first excavation phase, reaching a peak value of 466.46 kN. The minimum axial force in the cross-braces occurred during the sixth excavation phase, with a magnitude of 112.8 kN. The reason for the difference in the axial force between the two schemes lies precisely in the ingenious role of the reserved core soil.

A comparative analysis of the peak axial forces in the crossbracing under the BZL1 and BZL2 schemes is shown in Figure 19. When the BZL2 scheme was employed to excavate the foundation pit, the axial force absorbed by the cross braces was lower. This advantage was evident only during the first and sixth excavation stages. This is because the excavation procedures for steps 8 to 11 are identical

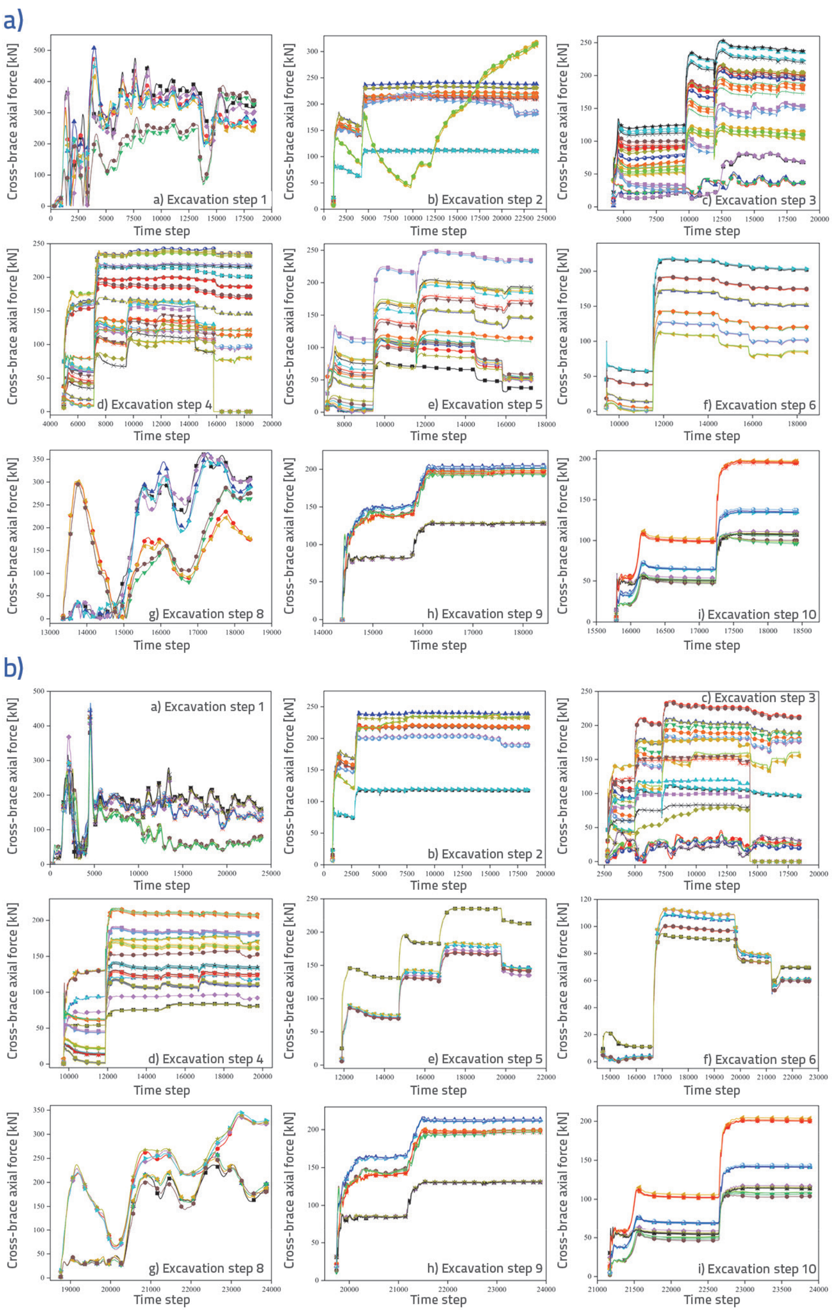

Figure 18. Variation patterns of lateral bracing axial forces at each monitoring point: a) BZL1 Programme; b) BZL2 programme

in both schemes; hence, the peak axial forces in the cross-bracing are essentially consistent. When the BZL2 scheme was employed to excavate the foundation pit, the peak axial force in the cross-braces reduced by up to 48.14 % compared to that under the BZL1 scheme. Moreover, when the BZL2 scheme was employed for excavating foundation pits, the stability of the retaining structure was enhanced.

Further analysis was conducted to understand the inherent mechanism of the reduction in the strut axial force under BZL2, in which the reserved core soil played an indispensable role. First, the reserved core soil directly bears part of the load and exerts a compression column effect. As a natural temporary support, the core soil directly bears a part of the horizontal earth pressure through its own compressive strength, thereby reducing the proportion of the load transferred to the transverse struts. Second, the reserved core soil restricts the propagation of the plastic zone. The core soil provides lateral restraint to the surrounding rock on both sides, reducing the overall deformation of the surrounding rock, and thereby decreasing the total pressure acting on the support system. Third, the reserved core soil blocks the stress transfer path. The core soil divides the continuous excavation face into discontinuous independent zones and blocks or weakens the direct transfer channels of the surrounding rock stress to the transverse struts, resulting in decentralised and localised loads on the struts. Finally, the reserved core soil suppresses the development of time-dependent deformation. The core soil slows the stress release rate of the surrounding rock, effectively constraining creep and relaxation deformation during the unexposed period before support installation and preventing a continuous increase in subsequent loads.

Based on a comprehensive analysis of the ground settlement and transverse strut axial force, it can be inferred that the BZL2 excavation scheme delivered a superior load control effect under the conditions of this study. However, it is necessary to discuss the applicability and limitations of the reserved core-soil method.

In terms of the applicable conditions, the reserved core soil method is suitable for rock masses or stiff soils with a certain self-stability capacity. The core soil must possess sufficient compressive strength to resist lateral loads. In soil layers with extremely poor self-stability, such as fluid-plastic soft soil, saturated sand, and soft clay with high water content, the reserved core soil may fail to maintain its stability and even become a potential safety hazard. Under these circumstances, foundation reinforcement and other construction methods must be adopted.

Regarding the limitations of the excavation scale, in the reserved core soil scheme, the foundation pit width must meet certain requirements. When the width is too small (e.g., < 10 m), the size of the core soil is restricted, making it difficult to achieve the desired effect. When the width is too large (e.g., > 60 m), the spacing between the excavation surfaces on both sides of the core soil becomes excessive, weakening the stress shadow effect.

The width, height, and slope of the reserved core soil are significantly sensitive to the control. For practical applications, an optimal design should be developed based on the geological conditions and geometric characteristics of the foundation pit. In addition, utilising the reserved core soil increases the construction procedures and may prolong the construction period. Technical and economic comparisons should be made based on the specific conditions in practical engineering applications.

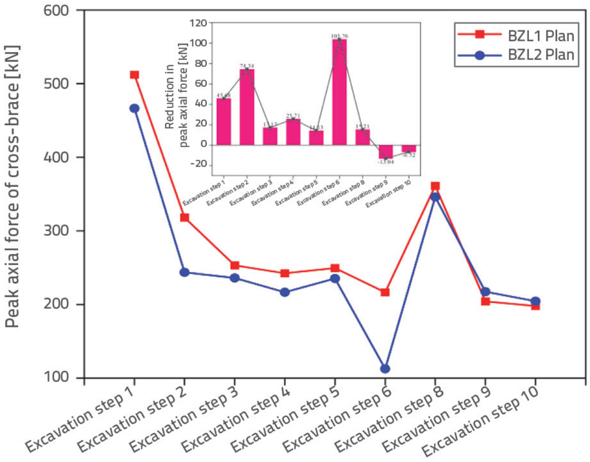

Figure 19. Comparison of the reduction in transverse bracing axial force between schemes BZL2 and BZL1

5. Conclusion

The reliability of the model and its parameters is a prerequisite for validating numerical simulation results. Based on the available monitoring data, the prediction error of the ground surface settlement under Scheme BZL1 calculated using the numerical simulation model was 13.84 %, indicating that the model has acceptable prediction capability under this specific condition.

A combined control method of "reserved core soil + symmetrical excavation" (Scheme BZL2) is proposed. The asymmetric disturbance of the unloading path of the surrounding rock is suppressed by actively retaining the central rock pillar. The engineering risk analysis shows that when the conventional excavation scheme (BZL1) is adopted, the plastic zone of the surrounding rock develops fully. The stress on the support structure approaches its critical yield point, resulting in a significant risk of instability. In contrast, when the foundation pit was excavated using Scheme BZL2, the peak cumulative ground settlement was reduced by up to 56.7 %. The ground settlement of buildings (structures) near survey lines 2–8 was significantly reduced, which effectively controlled the engineering risk within the safety threshold.

The peak axial force of the transverse struts when the foundation pit is excavated using Scheme BZL2 can be reduced by up to 48.14 % compared with that under Scheme BZL1. This indicates that the axial force acting on the transverse struts under the BZL1 scheme is significantly greater than that under the BZL2 scheme. The BZL2 scheme effectively reduces the loading level of the supporting structure. Based on a comprehensive analysis of the ground settlement and transverse strut axial force, the BZL2 excavation scheme was found to deliver a superior load control effect under the conditions of this study. However, for sensitive areas (such as Zones ① and ③ of Line 7), a real-time monitoring system should be established to realise a dynamic feedback design and information-based construction to further avoid engineering risks. Quantitative verification combining the design bearing capacity and safety factor is still required to determine whether the transverse struts approach the ultimate bearing state and to clarify their specific safety margins.

(4) The numerical simulation method employed in this study had certain limitations that require further investigation. For example, the model and its parameters must be verified comprehensively and systematically. The influence laws of water pressure variation, anisotropy of rock and soil mass, dynamic disturbance on ground surface settlement, and internal force of support structures must be investigated further.

Acknowledgments

This study was supported by Research on Key Technologies for Green and Intelligent Construction Control of Super-Large Deep Excavation Pits at Cross-Transfer Metro Stations for Chongqing Rail Transit Line 17 (DJTL-YBXM-2024-03).

REFERENCES

[1] Han, M., Chen, X.S., Jia, J.Q.: Analytical solution for displacement-dependent 3D earth pressure on flexible walls of foundation pits in layered cohesive soil, Acta Geotechnica, 19 (2024) 8, pp. 5249-5275, https://doi.org/10.1007/s11440-024-02226-x.

[2] Wang, Y.X., Guo, S.M., Tong, H.Z., Guo, P.P., Wu, W.B., Lu, M.M., Li, H.: Stability and failure probability analysis of super-large irregularly shaped deep excavation in coastal area considering spatial variability in soil properties, Journal of Asian Architecture and Building Engineering, 24 (2025) 6, pp. 5203-5219, https://doi.org/10.1080/13467581.2024.2409787.

[3] Hong, L., Wang, X.Y., Zhang, W.A., Li, Y.Q., Zhang, R.H., Chen, C.X.: System reliability-based robust design of deep foundation pit considering multiple failure modes, Geoscience Frontiers, 15 (2024) 2, pp. 101761, https://doi.org/10.1016/j.gsf.2023.101761.

[4] Ma, A.Y., Wang, W.Y., Zhu, W.X., Xu, Z.H., Ye, G.L.: Sensitivity analysis and application of the Shanghai model in ultra-deep excavation engineering, Geotechnics, 5 (2025) 1, https://doi.org/10.3390/geotechnics5010006.

[5] Zhang, Y., Zeng, Y.: Symmetric and asymmetric failure mechanism of deep tunnel excavation under complex environmental conditions, Symmetry, 17 (2025) 3, https://doi.org/10.3390/sym17030416.

[6] Zhang, B., Xu, J., Shi, X., Chen, N., Dong, Y., Wei, H., Wang, P.: Analysis of force characteristics of "pile-wall" structure based on elastic foundation beam method, GRAĐEVINAR, 77 (2025) 12, pp. 1201-1212, https://doi.org/10.14256/JCE.4134.2024.

[7] Chen, G., Zhang, X.H., Zhang, S.J., Huang, F., Xiao, H., Ma, H.Z., Luo, L.N., Bao, H.: Response monitoring and analysis in deep foundation pit excavation: A case study in soft soil at subway tunnel intersections, Buildings, 13 (2023) 5, pp. 1286, https://doi.org/10.3390/buildings13051286.

[8] Wang, S.H., Yang, B., Dong, F.R., Maxim, M., Zhang, Z.: Determination of the influence of the disturbance caused by traversing cross-type deep foundation pit excavations, Sustainability, 15 (2023) 2, pp. 1130, https://doi.org/10.3390/su15021130.

[9] Shi, H., Jia, Z.L., Wang, T., Cheng, Z.Q., Zhang, D., Bai, M.Z., Yu, K.: Deformation characteristics and optimization design for large-scale deep and circular foundation pit partitioned excavation in a complex environment, Buildings, 12 (2022) 9, pp. 1292, https://doi.org/10.3390/buildings12091292.

[10] Li, Y., Ma, Z.G., Gao, F.R., Gong, P., Gong, Z.Q., Li, K.L.: Deformation characteristics of a deep subway foundation pit in hard rock strata under a delayed supporting condition, Shock and Vibration, (2023), pp. 5155504, https://doi.org/10.1155/2023/5155504.

[11] Liang, J.M., Su, W.J., Liu, T.J., Wu, H.F., Lu, L.L., Zhong, H.S., Zhou, S.Y.: Analysis of large deformation characteristics of deep foundation pit at a subway station constructed by the tunnel-before-station method, European Journal of Environmental and Civil Engineering, 29 (2025) 16, pp. 3800-3827, https://doi.org/10.1080/19648189.2025.2527412.

[12] Li, G.C., Li, Q.M., Wang, J., Dong, J.M., Sun, Q.: The deformation characteristics of a 40-m-deep excavation supported by a suspended diaphragm wall in rock and soil composite ground, KSCE Journal of Civil Engineering, 26 (2022) 3, pp. 1040-1050, https://doi.org/10.1007/s12205-021-1810-2.

[13] Ding, H.B., Wang, X.P., Tong, L.H., Lu, Q., Xu, C.J., Guang, L.X.: Performance of isolation piles in protecting subway tunnels adjacent to foundation pits: Experimental and numerical investigations, Tunnelling and Underground Space Technology, 156 (2025), pp. 106221, https://doi.org/10.1016/j.tust.2024.106221.

[14] Fu, Y.B., Wang, B.L., Wu, H., Chen, X.S., Sun, X.H., Bian, Y.W., Shen, X.: Theoretical analysis on horizontal rectification of tunnel near deep foundation pit by grouting, Tunnelling and Underground Space Technology, 133 (2023), pp. 104977, https://doi.org/10.1016/j.tust.2022.104977.

[15] Ge, C.H., Li, P.F., Zhang, M.J., Ze, L.: Bearing capacity of High Bolt-Screw (HBS) active joints for prestressed internal bracing in subway excavations, Tunnelling and Underground Space Technology, 157 (2025), pp. 106251, https://doi.org/10.1016/j.tust.2024.106251.

[16] Qi, Y.C., Jia, F., Li, W.J., Shi, L., Qin, X.C., He, Y.W., Li, S.Y.: Optimization and energy consumption analyses of the support system of a super large deep foundation pit in the Xi'an Metro, Environmental Earth Sciences, 83 (2024) 5, pp. 140, https://doi.org/10.1007/s12665-024-11459-8.

[17] Chen, P., Liu, X., Cao, G., He, Y., Xu, A.: Deformation control for a five-story deep excavation, GRAĐEVINAR, 77 (2025) 7, pp. 699-708, https://doi.org/10.14256/JCE.4224.2024.

[18] Zhao, J.P., Wang, X.Y., Tan, Z.S., Zhang, X.B., Xiao, X.: Excavation optimization for asymmetrical deep foundation pits adjacent to subway stations: Deformation control and safety enhancement, International Journal of Geomechanics, 25 (2025) 12, pp. 05025010, https://doi.org/10.1061/IJGNAI.GMENG-11305.

[19] Zhang, W.S., Yuan, Y., Long, M., Yao, R.H., Jia, L., Liu, M.: Prediction of surface settlement around subway foundation pits based on spatiotemporal characteristics and deep learning models, Computers and Geotechnics, 168 (2024), pp. 106149, https://doi.org/10.1016/j.compgeo.2024.106149.

[20] Wu, B., Wan, Y.J., Xu, S.X., Zhao, C.X., Liu, Y., Zhang, K.: A multi-source intelligent fusion assessment method for dynamic construction risk of subway deep foundation pit: A case study, Sustainability, 15 (2023) 13, pp. 10162, https://doi.org/10.3390/su151310162.

[21] Wei, G., Feng, F.F., Cui, Y.L., Wang, X.Q., Diao, H.G., Wu, Y.: Research on the influence of foundation pit excavation on the lateral force and deformation of side shield tunnels based on full-scale experiments, Tunnelling and Underground Space Technology, 140 (2023), pp. 105236, https://doi.org/10.1016/j.tust.2023.105236.

[22] Xu, S.T., Xu, J.M.: Prediction of buildings' settlement induced by metro station deep foundation pit construction, Applied Sciences, 14 (2024) 5, pp. 2143, https://doi.org/10.3390/app14052143.

[23] Liu, Y., Huang, L., Tang, X.L., Xue, Y.B., Ke, W.B., Luo, Y., Guan, L.X.: Analysis of influence of cut-and-cover method on retaining structures and differential settlement in subway foundation pit construction, Applied Sciences, 15 (2025) 13, pp. 7520, https://doi.org/10.3390/app15137520.

[24] Xu, Y.Q., Zhao, Y.X., Jiang, Q.Q., Sun, J., Tian, C.X., Jiang, W.: Machine-learning-based deformation prediction method for deep foundation-pit enclosure structure, Applied Sciences, 14 (2024) 3, pp. 1273, https://doi.org/10.3390/app14031273.

[25] Gao, S., Zhao, W.G., Zhao, G.T., Wang, S.P., Xie, K.Z.: Numerical study on seismic performance of a prefabricated subway station considering the influence of construction process, Structures, 69 (2024), pp. 107218, https://doi.org/10.1016/j.istruc.2024.107218.

[26] Dong, Y., Luan, Y.Z., Wang, F., Luan, H.X., Jia, Z., Luan, H.X.: Monitoring and prediction of horizontal displacement of underground enclosure piles in subway foundation pits, ACS Omega, 8 (2023) 26, pp. 23389-23400, https://doi.org/10.1021/acsomega.2c00582.

[27] Hoek, E.: Hoek-Brown failure criterion – 2002 edition, Proceedings of the Fifth North American Rock Mechanics Symposium, 1 (2002), pp. 18-22.

[28] Sonmez, H., Ulusay, R.: Modifications to the geological strength index (GSI) and their applicability to stability of slopes, International Journal of Rock Mechanics and Mining Sciences, 36 (1999) 6, pp. 743-760, https://doi.org/10.1016/S0148-9062(99)00043-1.

[29] Yang, Y.M., Jiang, N., Yao, Y.K., Zhou, C.B., Meng, X.Z., Zhao, X.: Characteristics of stress concentration distribution in layered surrounding rock tunnels under dynamic and static loads, Journal of Zhejiang University (Engineering Edition), (2025), pp. 1-14.